

# PCCP

Accepted Manuscript

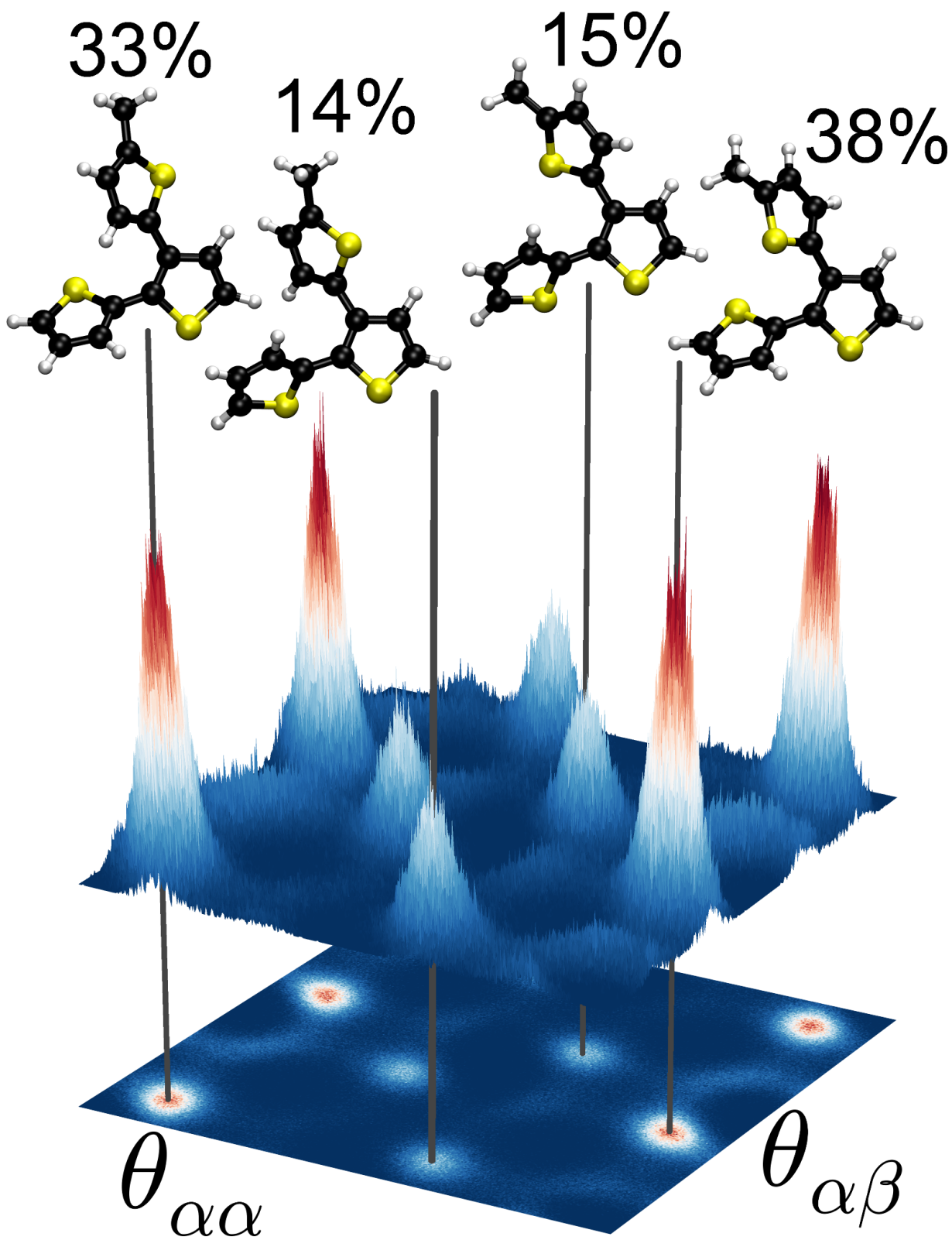


This is an *Accepted Manuscript*, which has been through the Royal Society of Chemistry peer review process and has been accepted for publication.

*Accepted Manuscripts* are published online shortly after acceptance, before technical editing, formatting and proof reading. Using this free service, authors can make their results available to the community, in citable form, before we publish the edited article. We will replace this *Accepted Manuscript* with the edited and formatted *Advance Article* as soon as it is available.

You can find more information about *Accepted Manuscripts* in the [Information for Authors](#).

Please note that technical editing may introduce minor changes to the text and/or graphics, which may alter content. The journal's standard [Terms & Conditions](#) and the [Ethical guidelines](#) still apply. In no event shall the Royal Society of Chemistry be held responsible for any errors or omissions in this *Accepted Manuscript* or any consequences arising from the use of any information it contains.



Averaged IR and Raman spectra are calculated using a method based on MD sampling, showing clear improvement over Boltzmann averaging.

# A Combined MD/QM and Experimental Exploration of Conformational Richness in Branched Oligothiophenes

Jonas Sjöqvist<sup>1</sup>, Rafael C. González-Cano<sup>2</sup>, Juan T. López Navarette<sup>2</sup>, Juan Casado<sup>2</sup>, M. Carmen Ruiz Delgado<sup>2</sup>, Mathieu Linares<sup>1</sup>, and Patrick Norman<sup>1\*</sup>

*<sup>1</sup>Department of Physics,  
Chemistry and Biology,  
Linköping University,  
SE-581 83 Linköping, Sweden*

*and*

*<sup>2</sup>Department of Physical Chemistry,  
University of Málaga,  
29071-Málaga, Spain*

(Dated: October 5, 2014)

## Abstract

Infrared (IR) absorption and vibrational Raman spectra of a family of branched oligothiophenes have been determined experimentally as well as theoretically. The molecular spectra have been compared to those of the linear analogues, with identification made of spectral features due to structural properties that are valued in organic solar cell applications. The theoretical spectra have been obtained through a newly developed method in which individual conformer spectra, calculated at the time-dependent DFT level in this work, are weighted by statistics extracted from classical molecular dynamics trajectories. The agreement with experiment for the resulting averaged spectra is at least as good as, and often better than, what is observed for Boltzmann-weighted spectra. As the weights are available before the costly step of spectrum calculation, the method has the additional advantage of enabling efficient approximations. For simulating the molecular dynamics of the studied  $\alpha,\beta$ -linked thiophenes and 2-methylthiophenes, high quality parameters have been derived for the CHARMM force field. Furthermore, the temperature dependence of the IR and Raman spectra have been investigated, both experimentally and theoretically.

Keywords: organic solar cells, time-dependent density functional theory, CHARMM, IR spectroscopy, Raman spectroscopy

## I. INTRODUCTION

Vibrational infrared (IR) absorption and Raman scattering spectroscopies are universally employed for the characterization of molecular and electronic structures, offering high sensitivity and delivering experimental data directly related to atoms and their molecular bonds.<sup>1–5</sup> For instance, in  $\pi$ -conjugated systems, the modifications in intensity and frequency of the bands associated with C=C/C–C stretching vibrations provide valuable information about conformational and structural factors that could affect the  $\pi$ -electronic delocalization.<sup>6–11</sup> Furthermore, as the chain conformation is highly sensitive to temperature, the temperature dependence of Raman and IR spectra is used to provide additional information about the changes in the molecular conformational properties. Since the performance of organic electronic devices is strongly dependent not only on the molecular structure and conformation of individual chains but also on interchain aggregation,<sup>12–15</sup> the information provided by vibrational spectroscopies at both the single- and supra-molecular levels is of particular relevance.

Three-dimensional (3D) oligothiophenes and polythiophenes have attracted a great deal of research interest in recent years due to their application in organic photovoltaics.<sup>16–18</sup> For instance, highly soluble dendrimers with up to 90 covalently linked thiophene rings synthesized by Bäuerle *et al.* showed solar cell efficiencies of up to 1.7%.<sup>16,17</sup> More recently, Ludwigs *et al.* prepared soluble hyperbranched polythiophenes with solar cell efficiencies close to 0.6%.<sup>18</sup> Two improvements are achieved in these 3D architectures when compared to their homologous linear systems: (1) better solubility that could facilitate processing and (2) more isotropic optoelectronic properties and larger contact surfaces for donor–acceptor interactions.<sup>19</sup> Some of us have recently investigated the interplay between  $\alpha,\alpha$ - and  $\alpha,\beta$ -conjugation in electronic and photophysical properties of different branched oligothiophenes as models for dendrimeric materials.<sup>20,21</sup> The investigation of excited state properties and charged defects of molecular materials is crucial to get insight into their function in photovoltaic applications. In a recent work,<sup>21</sup> we found that the conjugation through the  $\alpha,\beta$ -path is more effective in the singlet and triplet excited states than in the ground state, which is also connected with important molecular structure differences regarding planarity and bond length alternation.

The presence of different conformers in a 2,2';3',2''-terthiophene molecule named B3T

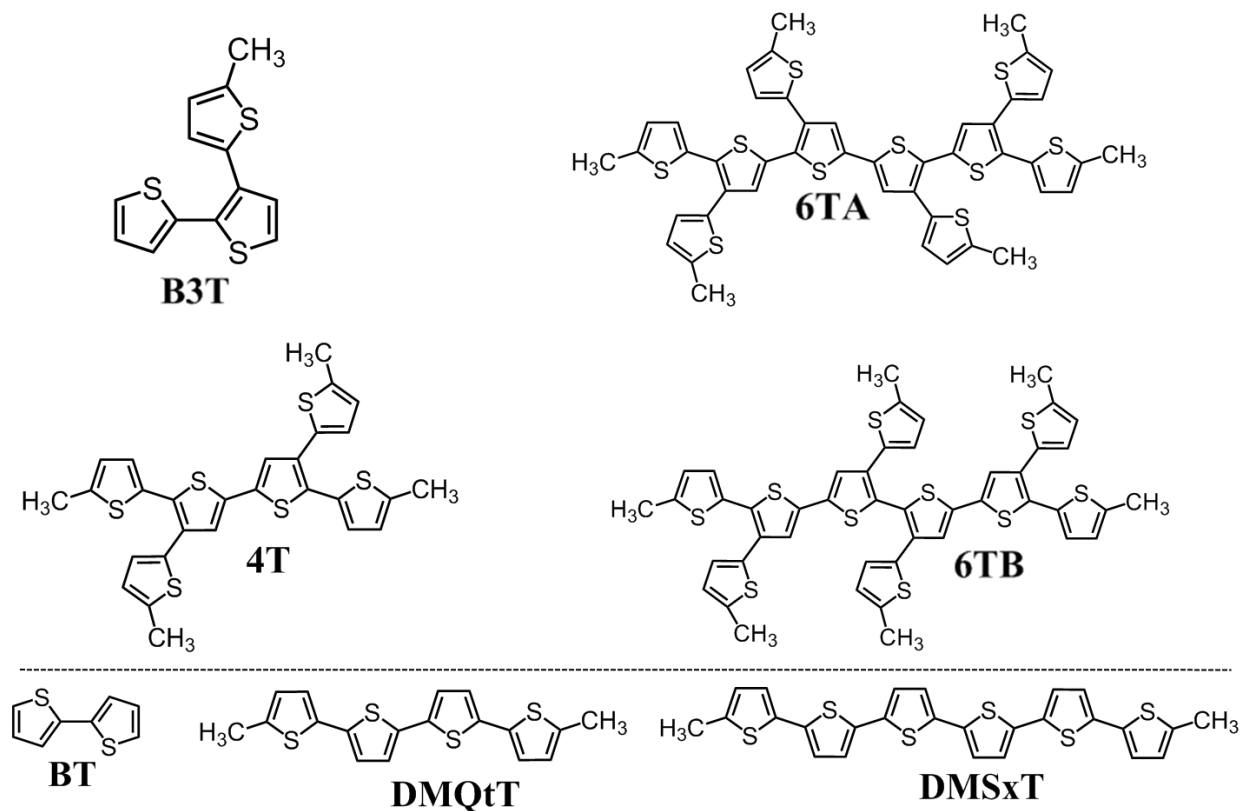


FIG. 1. Chemical structures and abbreviations for the compounds under study.

(see Fig. 1), the simplest building block of thiophene dendrimeric materials, was previously explored by us in a study using Raman spectroscopy.<sup>20</sup> DFT calculations predicted the existence of four minimum energy conformers in a small energy window of less than 0.7 kcal/mol. These were characterized on an individual basis as to obtain a final Raman spectrum in terms of a Boltzmann-weighted average. The resulting Raman spectrum showed a good agreement with experimental results except for a doublet band found in the region between 1472–1481  $\text{cm}^{-1}$ , caused by C–C stretching of the  $\beta$ -connected thiophene rings.<sup>20</sup> While the experimental spectrum showed two clear peaks in this region, the low-energy peak appears only as a weak shoulder in the theoretical spectrum. This could be attributed to the weighting used for the individual spectra of the four conformations as two of them contribute to the low-energy peak while the other two contribute to the high-energy peak. It was shown that by tuning the weight for the most conjugated all-*trans* conformation to 50% while maintaining the relative weights for the other three conformers, it was possible to more accurately reproduce the relative intensities of the experimental spectrum.<sup>20</sup>

With the intent to find the underlying reasons for the observed discrepancies between theory and experiment, we will in the present work improve on the microscopic description of the B3T system under the given experimental conditions. The Boltzmann weights, rather than the computational approach itself, are believed to be the source of the observed errors in the theoretical calculations. While the experimental measurements are obtained for the pure liquid, the calculations referred to a vacuum situation and it is of course possible that the presence of surrounding molecules causes conformational energy shifts. Given the sensitivity of Boltzmann statistics to conformer energetics as well as the rich dihedral dynamics in the oligomeric system, we decided to settle for nothing less than a direct and explicit description of the environment based on molecular dynamics (MD) simulations. Previous studies on luminescence properties of oligothiophenes have demonstrated that a highly accurate description of the chromophore dynamics in solution can be achieved with classical force fields that are carefully tuned against first-principles calculations.<sup>22,23</sup> In the present work, we will introduce MD simulations in calculations of infrared and Raman spectra of gas phase samples and pure liquids. This will enable us to pinpoint the conformational effect of the environment in the experiment and thereby address the previously observed discrepancies between theory and experiment.<sup>20</sup> This computational design strategy is also suitable to address large systems for which the technique of conventional Boltzmann averaging is hampered by the large number of conformers. We will illustrate this aspect by addressing three extended systems, based on four- and six-membered  $\alpha,\alpha$ -chains, named 4T, 6TA and 6TB, shown in Fig. 1.

In summary, herein we explore the conformational flexibility of a series of branched oligothiophenes using a joint experimental and theoretical vibrational study. Raman and IR spectroscopies are used to detect changes in the molecular conformation upon branching and to derive information about the type of electronic interactions that occur between the  $\alpha,\alpha$ -conjugated backbone and the  $\beta$ -linked thienyl units. A comparison with the properties of their linear analogues,  $\alpha,\alpha$ -bithiophene (BT), dimethyl tetrathiophene (DMQtT) and dimethyl sexithiophene (DMSxT) is proposed. A new method for the calculation of the vibrational spectra is developed based on molecular dynamics simulations. The resulting theoretical predictions successfully provide a thorough comprehension of the vibrational properties of branched oligothiophenes, which until now has represented a challenge in the field of spectroscopy and molecular modeling.

## II. METHODOLOGY

### A. Force field parameterization

For this work, where conformational statistics are studied for highly flexible molecules, it is crucial that the MM force field accurately describes the motion of the molecules, with the parameters defining the torsional barriers between the thiophene rings being of particular importance. A high quality set of parameters for  $\alpha,\alpha$ -linked thiophenes has already been developed<sup>22,23</sup> for the CHARMM22 force field,<sup>24</sup> making it a suitable choice for this study. However, no description of  $\beta$ -linked thiophenes exists, nor any for methyl groups attached in the  $\alpha$ -position on thiophenes. Therefore, before any MD simulations could be run, a number of force field parameters needed to be derived. In order to describe the  $\alpha,\beta$  connection between thiophene rings, two additional atom types were introduced to the force field, C5RPB and C5RB, corresponding to the bonded  $\alpha$  and  $\beta$  carbons, respectively. The structure of the molecules and the atom types used are available in Fig. 1 of the supplementary information. In total, two bond stretching parameters, four angle bending parameters and two torsional parameters needed to be created, with additional missing parameters taken directly from the equivalent C5RP and C5R parameters. The parameterizations were performed for each parameter separately and done by fitting to zero temperature optimized structures and potential energy curves obtained at the DFT level of theory.

### B. Molecular dynamics

Molecular dynamics simulations were run at room temperature for the four branched oligothiophenes, both in the gas and liquid phases. The gas phase dynamics were obtained by simulating a single molecule in a large periodic box while the liquid phase was simulated using a thermally equilibrated periodic box containing a large number of molecules. At regular intervals, the structures of the molecules were extracted and their conformations were determined. This was done by calculating the dihedral angles formed between a pair of bonded thiophene rings and identifying it as being either in the *cis* or *trans* position. For  $\alpha,\alpha$ -bonded thiophenes, any angle below 90 degrees, formed between the two sulfur atoms while looking through the carbon-carbon bond, is defined as *cis* while any angle at or above 90 degrees is defined as *trans*. The same definition is used for the  $\alpha,\beta$ -bonded thiophenes,

with the angle defined between the sulfur and the  $\alpha$ -carbon. Using these definitions, each molecular structure can be placed into a rough conformational category. This way, given that a long enough MD simulation is run, and a large enough number of structural samples are taken from this simulation, it is possible to obtain accurate statistics for the conformational distribution. In this work, we collected a total of one million molecular structures from each dynamics simulation, which, given the size and flexibility of the studied family of molecules, is more than enough to generate a representative conformational distribution.

### C. IR and Raman spectroscopy

We will work under the assumption that the coupling between vibrational and rotational motions can be neglected and that the experimental Raman spectrum is due to Stokes scattering. In addition, we will assume that any effects due to electrical and mechanical anharmonicities is small and can be accounted for by a mere scaling of vibrational frequencies with a standard, functional-dependent, factor. In other words, we assume that the theoretical approach for calculating individual spectra is sound and that the source of the observed errors lies in the Boltzmann weighting.

The theoretical spectra in this work are all weighted averages, based on individual spectra calculated for the optimized structures of all possible conformations for the relevant molecule. The conformations are defined as in Section II B, with each pair of bonded thiophene rings being classified as either in the *cis* or *trans* position. For B3T, which is asymmetrical, there are 4 possible conformations, while for the remaining symmetrical molecules there are  $2^{N-2} + 2^{N/2-1}$  possible conformations, where  $N$  is the number of thiophene rings. As such, there are 20 conformations for 4T and 272 conformations for both 6TA and 6TB. Starting positions for the geometry optimizations were extracted from the MD trajectories by locating the most planar example of each conformation. Planarity was in this case defined by the expression

$$P = \sum_i \frac{||\theta_i| - 90|}{90}, \quad (1)$$

where  $\theta_i$  is the dihedral angle between two thiophene rings and  $i$  sums over all such angles. All IR and Raman spectra were calculated in the double-harmonic approximation, see Ref. 25 for a detailed presentation of the pertinent expressions.

### III. COMPUTATIONAL DETAILS

All optimized structures and potential energy curves used in the force field parametrization were obtained using the Gaussian 09 program.<sup>26</sup> For these reference calculations, the B3LYP functional was used together with the aug-cc-pVTZ<sup>27,28</sup> basis set. Bond lengths were scanned within  $\pm 0.2$  Å of the optimized length and at 0.05 Å intervals. Bond angles were scanned within  $\pm 5^\circ$  of the optimized angle and with a step of  $1^\circ$ . For the torsional angles, a relaxed scan covering a  $180^\circ$  rotation was performed at steps of  $15^\circ$ . The resulting force field parameters are presented in Table I.

TABLE I. Optimized CHARMM force field parameters.  $K_b$  is given in kcal/mol/Å<sup>2</sup>,  $b_0$  in Å,  $K_\theta$  in kcal/mol/rad<sup>2</sup>,  $\theta_0$  in degrees,  $K_\chi$  in kcal/mol and  $\delta$  in degrees.

Bond type	$K_b$	$b_0$	
CT-C5R	340.0	1.497	
C5RB-C5RPB	360.0	1.458	
Angle type	$K_\theta$	$\theta_0$	
C5RB-C5RPB-S5R	95.0	122.0	
C5R-C5RB-C5RPB	70.0	124.0	
C5RB-C5RPB-C5R	70.0	128.0	
C5RPB-C5RB-C5RP	70.0	128.0	
Dihedral type	$K_\chi$	$n$	$\delta$
HA-CT-C5R-S5R	0.100	3	0.0
HA-CT-C5R-C5R	0.000	3	0.0
C5R-C5RB-C5RBP-S5R	0.435	2	180.0
	0.075	4	0.0
C5R-C5RB-C5RBP-C5R	0.435	2	180.0
	0.075	4	0.0
C5RP-C5RB-C5RBP-S5R	0.435	2	180.0
	0.075	4	0.0
C5RP-C5RB-C5RBP-C5R	0.435	2	180.0
	0.075	4	0.0

The Gromacs program<sup>29</sup> was used for all molecular dynamics simulations, employing the CHARMM force field<sup>24</sup> in conjunction with additional parameters for the description of polythiophenes<sup>22,23</sup> as well as those created in this work. The charges are taken from the PCFF force field<sup>30,31</sup> and are available in Fig. 1 of the supplementary information. All simulations were performed using the Nosè–Hoover thermostat<sup>32–34</sup> and NPT simulations were performed either solely using the Parrinello–Rahman barostat<sup>35</sup> or using the Berendsen barostat<sup>36</sup> for an initial rough equilibration, followed by further simulations using the Parrinello–Rahman barostat. For the gas phase simulations, a single MD simulation was run for a single molecule in a periodic cubic box with side length 10 nm. After an initial equilibration of 1 ns the simulations were run for 10  $\mu$ s, with structural sampling performed every 10 ps, resulting in a total of one million molecular structure samples. For the liquid phase simulations, an initial geometry containing 400 molecules was generated using the Packmol program.<sup>37</sup> Starting from this geometry, a 20 ps dynamic was run at a temperature of 600 K and using an NPT ensemble, followed by 500 ps dynamic at the same temperature but using an NVT ensemble. After this, an NPT dynamics was run at 300 K for as long as was needed for the density of the box to converge, which for the studied molecules meant simulation times between 1.5 and 5 ns. The resulting densities were found as 1240, 1260, 1295, and 1285 kg/m<sup>3</sup> for B3T, 4T, 6TA, and 6TB, respectively. Compared to the experimental density of 1553 kg/m<sup>3</sup> for the planar sexithiophene,<sup>38</sup> these densities appear reasonable considering the branched structures of the molecules. Starting from such a thermally equilibrated box, an NVT dynamic of 26 ns was run with structural samples taken every 10 ps, following the equilibration in the first nanosecond. This results in a total of 2500 sampled structures, each containing 400 individual molecules, giving a total of one million molecule structures.

IR and Raman spectra calculations, as well as the preceding geometry optimizations, were performed using the Gaussian program and with both the B3LYP functional as well as the Coulomb attenuated B3LYP (CAM-B3LYP)<sup>39</sup> functional. For these calculations the 6-31G\*\* basis set<sup>40,41</sup> was used. The final spectrum for each molecule was created as an average of the individual conformation spectra, weighted either by conformational statistics taken from the MD trajectories or by the Boltzmann weights, calculated as

$$P_i = \frac{e^{-\varepsilon_i/k_B T}}{\sum_j e^{-\varepsilon_j/k_B T}}, \quad (2)$$

where  $P_i$  is the weight for conformation  $i$ ,  $\varepsilon_i$  is the total energy including zero-point vibrations

in conformation  $i$ ,  $k_B$  is the Boltzmann constant and  $T$  is the temperature in Kelvin, which has been set to 300 K unless otherwise stated. All B3LYP spectra were scaled by a vibrational scaling factor of 0.961<sup>42</sup> and all CAM-B3LYP spectra were scaled by 0.942, which was obtained by a fit to experimental data.

#### IV. EXPERIMENTAL DETAILS

Fourier Transform (FT) Raman scattering spectra with 1064 laser excitation were recorded using a Bruker FRA 106/S instrument and a Nd:YAG laser source with excitation at  $\lambda = 1064$  nm, operating in a back-scattering configuration. The operating power for the exciting laser radiation was kept in the range of 450–1000 mW in all experiments. Samples were analyzed by averaging 500 scans with 4  $\text{cm}^{-1}$  spectral resolution. Raman scattering spectra with 532 laser excitation were also recorded using a Bruker Senterra dispersive Raman microscope equipped with a neon lamp and using a Nd:YAG laser with excitation at  $\lambda = 532$  nm. Samples were registered at low, room, and high temperatures in a variable-temperature Linkam accessory. The operating power for B3T was 5 mW for all temperatures and the samples were analyzed by averaging 20 scans with 4  $\text{cm}^{-1}$  spectral resolution. The operating power for 4T, 6TA and 6TB was 0.2 mW for all temperatures and the sample was analyzed by averaging 25 scans for 6TA and 100 scans for 4T and 6TB with 4  $\text{cm}^{-1}$  spectral resolution. Fourier transform infrared absorption (FT-IR) spectra were recorded on a Bruker Equinox 55 spectrometer. Compounds were ground to a powder and pressed into KBr pellets. Spectra were collected with a spectral resolution of 4  $\text{cm}^{-1}$ , and a mean of 50 scans were recorded. Interference from atmospheric water vapor and  $\text{CO}_2$  was minimized by purging the instrument with dry argon prior to data collection. Variable temperatures were reached by using a Specac P/N 21006 accessory with quartz windows and Graseby Specac temperature controller.

#### V. RESULTS AND DISCUSSION

##### A. Experimental IR and Raman spectra

For the branched systems under study, very similar Raman spectral profiles are obtained when using both 532 and 1064 nm laser excitation wavelengths because in both cases the

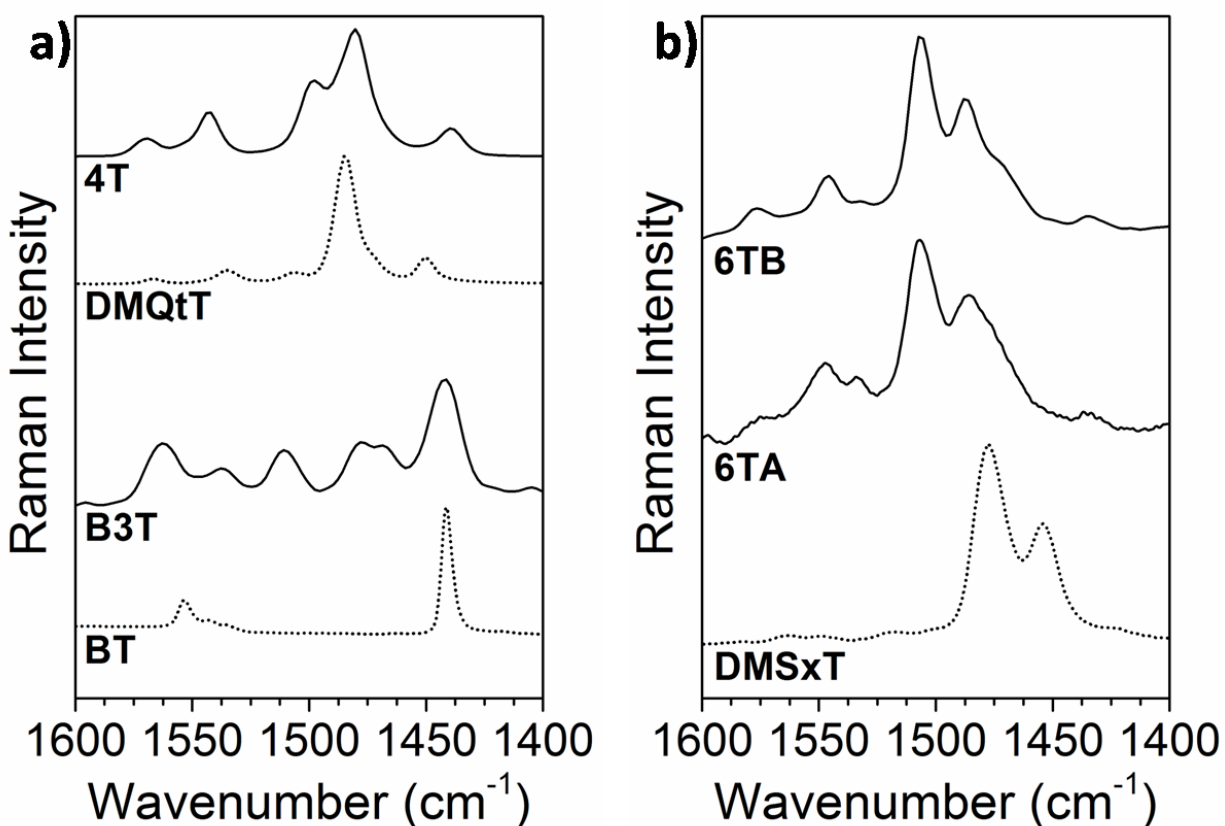


FIG. 2. Experimental FT-Raman spectra of (a) B3T, BT, 4T and DMQtT, and (b) 6TA, 6TB and DMSxT. Note that the solid lines shows the spectra of the branched systems and the dotted lines show the spectra of the linear systems.

samples are out of resonance Raman conditions with the HOMO–LUMO transitions.<sup>20,21</sup> In Fig. 2, we show the Raman spectra of the branched systems under study and, for reference, those of the linear  $\alpha,\alpha$ -conjugated homologues. An illustration of the chemical structure of all systems can be seen in Fig. 1. In comparison to those of the linear  $\pi$ -conjugated oligothiophenes, more complex Raman spectra are found for the branched oligothiophenes, with broader bands in the region between 1400–1600  $\text{cm}^{-1}$  attributable to specific symmetrical C=C/C–C vibrations along their  $\pi$ -conjugated backbones. This can be related to: (i) lack of molecular symmetry when going from the linear to the branched systems, (ii) increase of molecular flexibility upon  $\beta$ -thienyl substitution (i.e., presence of different conformers), and (iii) restricted electronic coupling of the  $\beta$ -linked thienyl rings and the  $\alpha$ -oligothiophene backbone. Besides displaying much broader and complex spectral profiles, the strongest

Raman scattering bands in the branched systems are largely upshifted when compared to the all- $\alpha$  conjugated homologue systems, e.g., the band at  $1477\text{ cm}^{-1}$  in DMSxT is shifted to  $1503\text{ cm}^{-1}$  in 6TA and  $1507\text{ cm}^{-1}$  in 6TB. This agrees well with the increased inter-ring distortion of the  $\alpha,\alpha$ -conjugated backbone upon insertion of the  $\beta$ -linked thienyl rings, which results in a decrease of the overall  $\pi$ -conjugation. Note that this up-shifting and broadening is more pronounced in the more distorted 6TB system due to the steric hindrance imparted by the two head-to-head inner  $\beta$ -linked thiophenes.

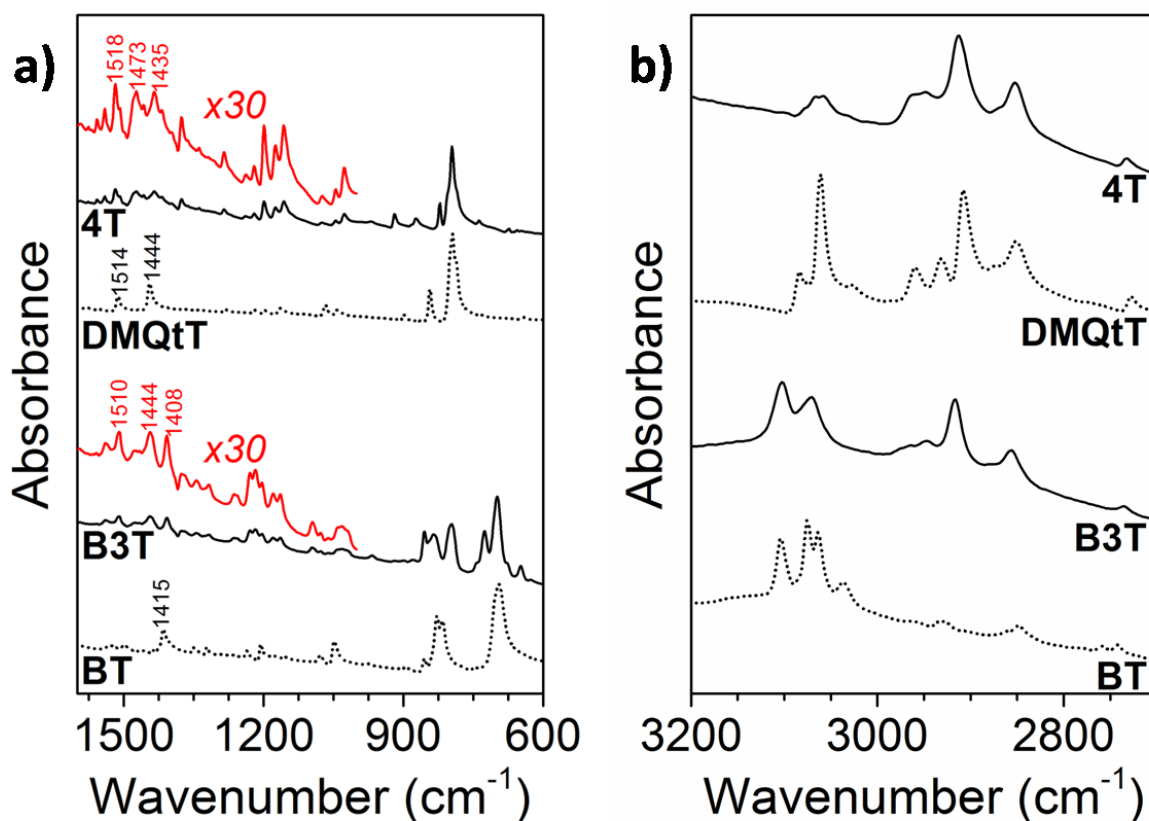


FIG. 3. Experimental infrared spectra of B3T, BT, 4T and DMQtT in (a) the  $1600\text{--}600\text{ cm}^{-1}$  region with a zoomed in version of the  $1600\text{--}1000\text{ cm}^{-1}$  region for B3T and 4T shown in red, and (b) the  $3200\text{--}2700\text{ cm}^{-1}$  region.

Fig. 3 displays the infrared spectra of B3T and 4T as well as their respective all  $\alpha$ -conjugated homologues BT and DMQtT. Although the out-of-plane  $\gamma(\text{C-H})$  bending vibrations, appearing near  $800\text{ cm}^{-1}$ , display the by far strongest infrared absorptions, the C-C/C=C stretching modes in the region between  $1000\text{--}1600\text{ cm}^{-1}$  also show moderate IR

activities for the branched systems. This can be explained by the sizeable fluxes of charge induced by the  $\beta$ -linked thienyl rings along the more distorted  $\alpha,\alpha$ -conjugated backbone in the branched systems which results in stronger IR-activities. Specifically, there is a large number of bands dominating the 1350–1550  $\text{cm}^{-1}$  infrared region that are not present in the linear systems. These bands are due to the antisymmetric and symmetric stretching modes of the aromatic C=C bonds, which shift moderately upward upon insertion of  $\beta$ -linked thienyl groups (from 1514 and 1444  $\text{cm}^{-1}$  in DMQtT to 1518, 1473 and 1435  $\text{cm}^{-1}$  in 4T). This indicates the existence of a vibrational coupling between the motions of the  $\alpha,\alpha$ -conjugated core and the  $\alpha,\beta$ -conjugated thienyl units. However, this effect does not result in an increase of the overall  $\pi$ -conjugation of the system, due to the larger distortions from coplanarity upon branching. In the high-energy region, all oligomers show characteristic bands around 3060–3100  $\text{cm}^{-1}$  that are assigned to stretching of C–H bonds in rings, and well-resolved peaks in the 2850–2970  $\text{cm}^{-1}$  region that are assigned to C–H stretching in the methyl groups. As the ratio of methyl groups increases for the branched system compared to their linear equivalents, the intensities of the absorptions due to these groups also increase. This can be clearly seen when comparing 4T to the linear  $\alpha,\alpha$ -conjugated DMQT, with the methyl stretching modes in 4T showing an increase in strength with respect to those due to C–H stretching. It is also interesting to note that 4T shows different multiplets at 3060  $\text{cm}^{-1}$  on the high-energy side of the band, associated with C–H stretching at the  $\beta$ -positions of the  $\alpha$ -coupled and  $\beta$ -coupled thienyl rings with different phases.

## B. Theoretical IR and Raman spectra of B3T

To give a visualization of the differences in dynamics between the gas and liquid phases of B3T, two-dimensional histograms, showing the distribution of the two dihedral angles formed between the thiophene rings,  $\theta_{\alpha\alpha}$  and  $\theta_{\alpha\beta}$ , are displayed in Fig. 4. In the histograms, the four conformations can easily be identified and it is evident that, in the liquid phase, the molecule is more likely to be found close to the optimized conformation structures. Based on this visualization, it is also possible to identify the pathways between the conformations as the brighter areas connecting the conformational regions. However, it is not possible to immediately identify whether there is any significant difference in the conformational distribution between the two phases. Using the method for categorizing conformations described

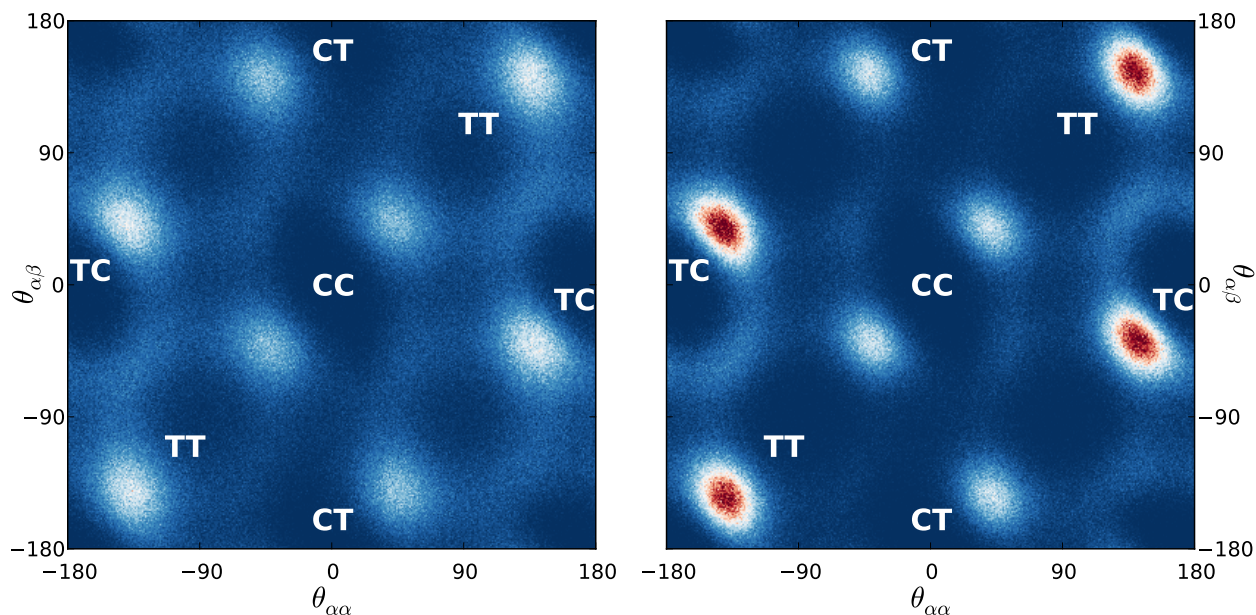


FIG. 4. Two-dimensional histograms showing the distribution of dihedral angles formed between thiophene rings found in the B3T MD simulations. The gas phase histogram is shown on the left and the liquid phase histogram on the right, with both being based on one million structures. Red indicates a high number of structures and blue a low number, with white in between.

in Section II B, it is found that there are noticeable differences between the distributions, with changes in weights between 4–6 percent. However, when compared to the B3LYP Boltzmann weights, as shown in Table II, we note differences that qualitatively alter the statistics. For instance, whereas the *trans-cis* (TC) conformation (i.e. *trans* conformation of the  $\alpha$ -linked bithiophene and *cis* conformation of the  $\beta$ -linked thiophene) contributes the most to a spectral average based on the MD statistics, the same conformation contributes the least when using the corresponding Boltzmann statistics. At first glance, this result appears very counterintuitive since the force field is parameterized against B3LYP energetics. But we must here remind ourselves that we are studying systems for which low-barrier dihedral motion plays an important role, and the systems therefore spend large portions of time far away from any of the local minima on the potential energy surface. Since Boltzmann weights are based solely on the energies found at the respective minima, they fail to correctly weight the time spent in the wider region around these precise points. This becomes particularly critical in a situation as encountered here, where conformations are nearly degenerate with relative energies of less than 1 kcal/mol.

TABLE II. Conformational distributions for B3T based on MD statistics and Boltzmann weights. The first letter of the conformation indicates whether the  $\alpha,\alpha$ -bonded rings are in the *cis* (C) or *trans* (T) position while the second letter does the same for the  $\alpha,\beta$ -bonded rings.

Conformation	MD statistics		Boltzmann weights	
	Gas	Liquid	B3LYP <sup>a</sup>	CAM-B3LYP
TC	32%	38%	15%	16%
TT	29%	33%	37%	38%
CC	20%	15%	16%	16%
CT	19%	14%	32%	30%

<sup>a</sup> The B3LYP weights reproduce the distribution reported in Ref. 20, with slight variations due to the inclusion of zero-point vibrations in the energy calculations.

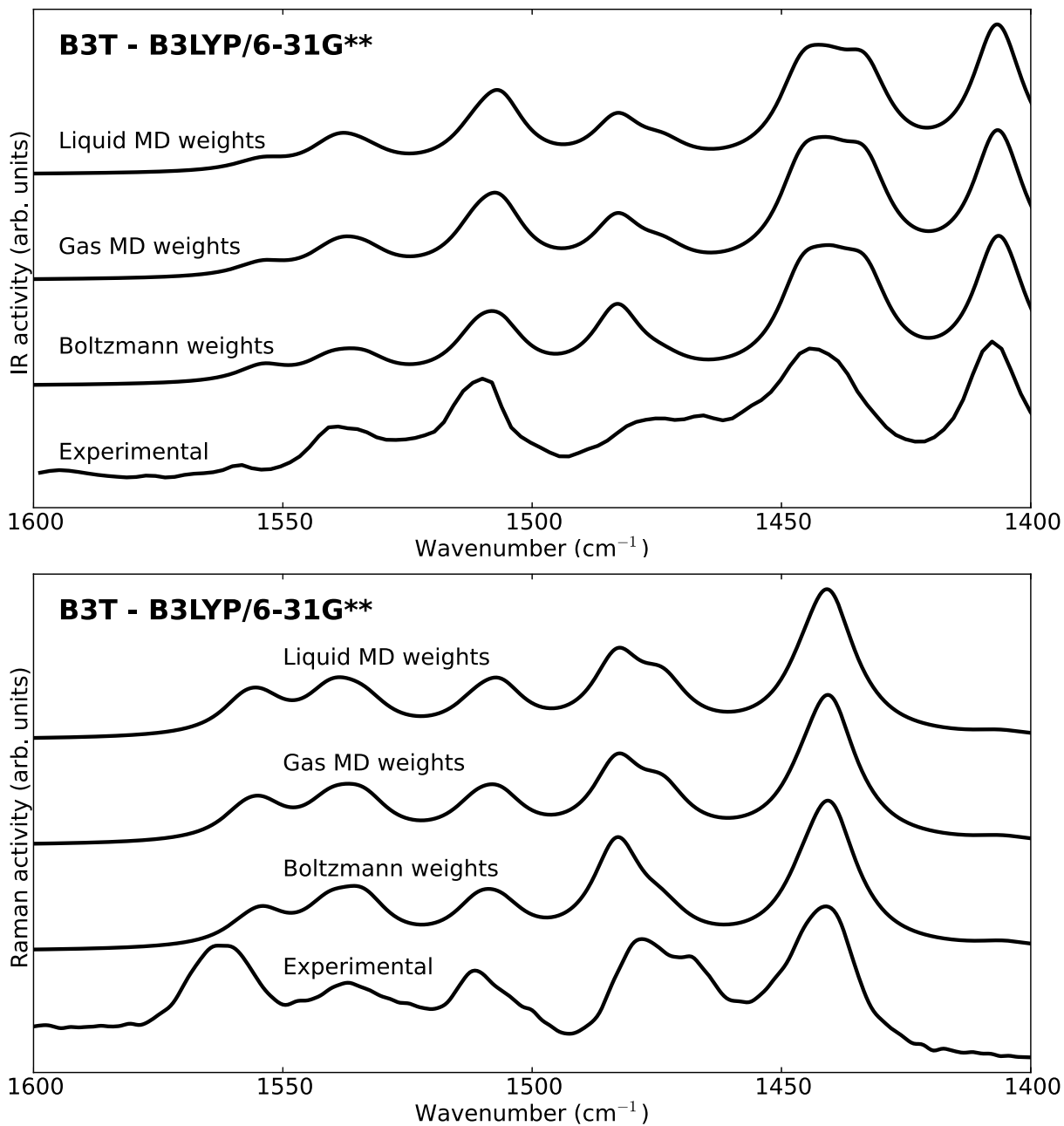


FIG. 5. Theoretical room temperature IR and Raman spectra for B3T compared to experiment. The experimental Raman spectrum is recorded at 532 nm.

Fig. 5 shows the theoretical IR and Raman spectra of B3T, as weighted by the two MD statistics as well as by the Boltzmann distribution found in Table II, along with the experimental spectrum. All theoretical spectra are based on the same individual conformational spectra, calculated at the B3LYP/6-31G\*\* level of theory, with only the weights differing. The B3LYP weighting recreates the previously calculated Raman spectrum, including the unsatisfactory description of the doublet band in the 1481–1472  $\text{cm}^{-1}$  region, associated with C–C stretching over the  $\beta$ -connected thienyl rings. This problem is remedied when using the weighting from the MD statistics, resulting in spectra that are in close agreement with the measurements. The only exception is found for the peak at 1555  $\text{cm}^{-1}$ , which, while slightly stronger for the MD weights, is underestimated in all averaged spectra. Study of the individual conformer spectra show that this peak is too weak in all cases, indicating that this discrepancy stems from the spectrum calculations, not the weights used to average them. The MD weights also produce better results for the IR spectrum, where there is a plateau in the 1481–1472  $\text{cm}^{-1}$  region of the experimental spectrum. In the Boltzmann weighted spectrum, this region contains a single peak, which remains in the MD weighted spectra, but weakened and joined by a second peak, creating a shoulder that more closely resembles the experiment. There does not, however, appear to be any significant difference between the gas and liquid phase spectra for neither IR nor Raman. This suggests that the inaccuracies when using the Boltzmann weighting stem from the approach itself and not from the fact that the energies are obtained in the gas phase. The MD weights, on the other hand, appear to give a much improved agreement with experiments. Indeed, for each calculated spectrum in this work, the MD weights give at least as good an agreement as, and in most cases better than, the Boltzmann weights, and as such, all subsequent theoretical spectra presented in the main article, with the exception of those found in the section about thermal dependence, will be obtained with weights based on liquid MD statistics. All spectra are, however, available with all different weightings in the supplementary information.

### C. Theoretical IR and Raman spectra of 4T, 6TA and 6TB

Applying the same methodology of using MD weights works well also for the mid-size 4T molecule, producing a B3LYP Raman spectrum that is in excellent agreement with the experimental results and an IR spectrum that is in acceptable agreement, as shown in Fig. 6.

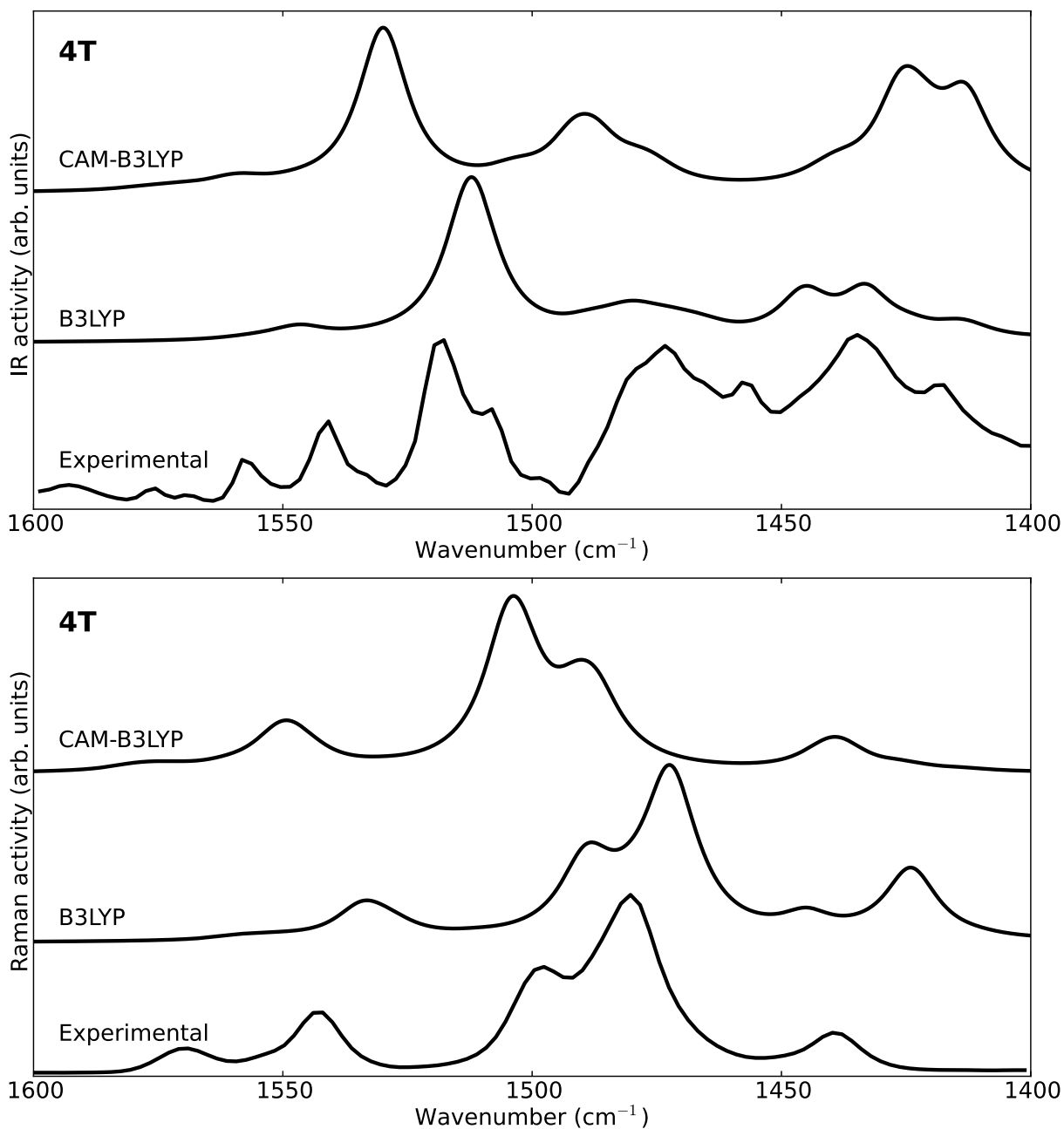


FIG. 6. Theoretical room temperature IR and Raman spectra for 4T, weighted by liquid MD statistics, compared to experimental IR and FT-Raman spectra.

However, this is not the case for the two larger molecules, as shown in Fig. 7. The B3LYP Raman spectrum of 6TA and 6TB bears almost no resemblance to the experimental data, indicating that there are severe problems in the theoretical description.

To find out why this theoretical description is inaccurate, several possible error sources

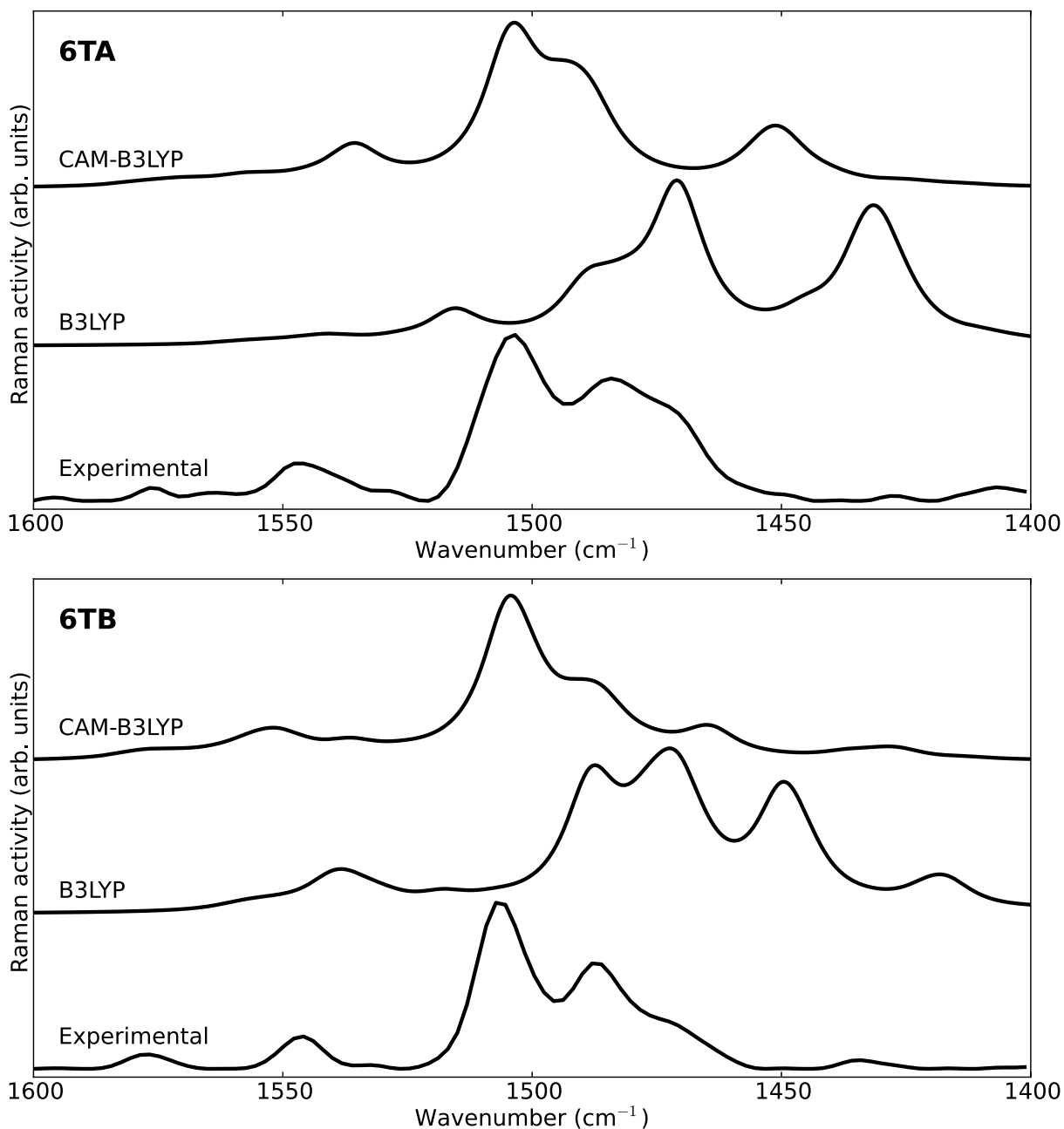


FIG. 7. Theoretical room temperature Raman spectra for 6TA and 6TB, weighted by liquid MD statistics, compared to experimental IR and FT-Raman spectra.

were investigated. As the calculated spectra for both 6TA and 6TB are the result of a weighted average of 272 conformations, it is possible that the problem lies in an inaccurate weighting, discrediting our proposed procedure of using MD weights. There is strong evidence for this not to be the case, however, as none of the spectra for the individual conformers

contain the components necessary to build a spectrum that better resembles the experimental one. The size of the basis set is also a possible source of errors, though this explanation is easily discarded with a straightforward basis set test. Using the larger 6-311G\*\* basis set only introduces slight changes to the positions and intensities of the peaks in the Raman spectrum, but retains the same general appearance as when calculated using the smaller basis set. A more likely source of error lies in the description of the electronic structure for our more extended systems, or in other words the choice of exchange-correlation functional. This assumption appears likely in view of the fact that the standard B3LYP functional is known to give an inaccurate description of electronic transitions and response properties (such as e.g. polarizabilities) in extended conjugated systems.<sup>43</sup> As the intensities of the peaks in the Raman spectrum depend on the derivative of the polarizability with respect to vibrational coordinates, such errors are likely to significantly alter the calculated spectra. The CAM-B3LYP functional attempts to remedy this by introducing a range separation, altering the amount of Hartree–Fock exchange based on the electron–electron separation distance. As is evident in the Raman spectra calculated using CAM-B3LYP for 6TA and 6TB, shown in Fig. 7, this appears to solve the problem, with a much improved experimental agreement. While no experimental measurements of IR spectra for 6TA and 6TB were made, theoretical spectra calculated both with B3LYP and CAM-B3LYP are available in Fig. 2 of the supplementary information.

As CAM-B3LYP has a short-range and long-range behavior, smaller molecules that fall within the short-range region should be described in a manner similar to B3LYP. As such, for B3T and 4T, which were both described well by B3LYP, we should not see any major spectral changes when using CAM-B3LYP. This is mostly true for B3T, showing relatively small changes in the positions and weights of the peaks, with the most noticeable difference being an overestimation of the strength of the peak found at  $1410\text{ cm}^{-1}$  in the IR spectrum (see Fig. 3 in the supplementary information). The same cannot be said for the 4T spectra, shown in Fig. 6, where the CAM-B3LYP IR spectrum remains largely unchanged as compared to the B3LYP calculation but the Raman spectrum has changed significantly. The intensities of the two main peaks have been switched, resulting in an incorrect spectral profile. It appears that the switch between short- and long-range in CAM-B3LYP occurs at a slightly too short distance to give a proper description of 4T, but works well for the smaller and larger molecules. Since it is possible to alter the parameters in CAM-B3LYP that govern

this switching behavior, it would most likely be possible to tune the CAM-B3LYP functional so that it gives a good description for all four molecules, but such a study lies outside the scope of this work.

#### D. Thermal dependence of the IR and Raman spectra

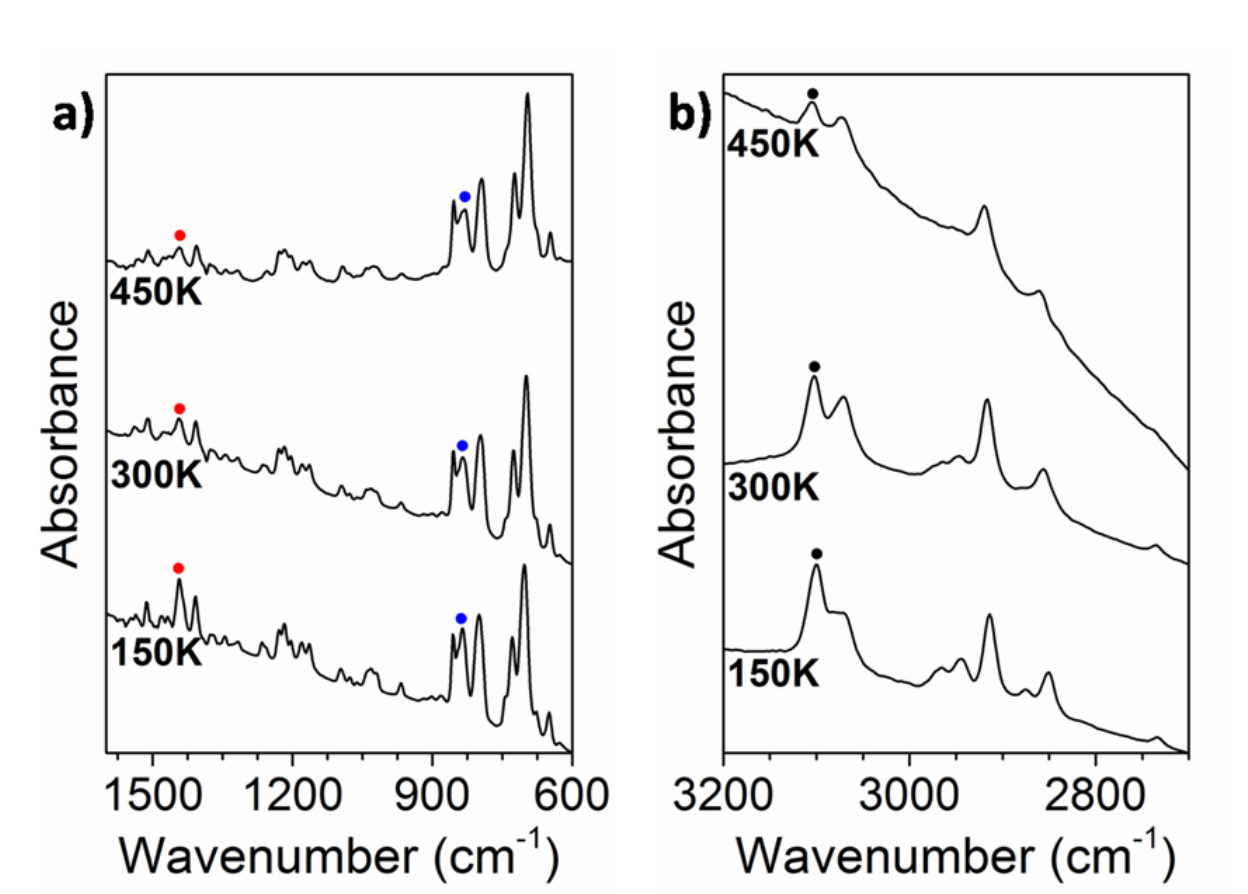


FIG. 8. Experimental infrared spectra of B3T at different temperatures. (a) The 1600–600 cm<sup>-1</sup> region; (b) the 3200–2700 cm<sup>-1</sup> region.

By raising or lowering the temperature of the system, it may be possible to introduce conformational changes. Infrared spectroscopy provides a simple way of detecting such changes. Therefore, it is of interest to study the temperature effect on the branched oligothiophenes, starting with the shortest branched system, B3T, as the simplest building block of such materials. In Fig. 8, we show temperature-variable infrared spectra of B3T. Contrary to what is found for the crystalline systems such as  $\alpha,\alpha$ -dimethyloligothiophenes,<sup>44</sup> the widths

of the IR bands neither substantially narrow nor split when lowering the temperature, which is consistent with the amorphous nature of the branched systems. However, some spectral changes are observed when the temperature is lowered: (i) The C=C stretching mode at  $1444\text{ cm}^{-1}$  (indicated as a red dot in Fig. 8) increases in intensity with the upsurge of a shoulder at lower frequencies associated with methyl bending vibrations; (ii) the out-of-plane C-H bending modes of the unsubstituted  $\alpha,\alpha$ -coupled thiophene at  $835\text{ cm}^{-1}$  (indicated as a blue dot in Fig. 8) increase in intensity and (iii) the stretching of the C-H modes at the  $\alpha$ - and  $\beta$ -positions of the unsubstituted  $\alpha,\alpha$ -coupled thiophene at  $3101\text{ cm}^{-1}$  (indicated as a black dot in Fig. 8) increase in intensity while those related to the  $\beta$ -linked thiophene at  $3070\text{ cm}^{-1}$  decrease in intensity. These spectral changes are related to a redistribution of the molecular conformations due to an increase of intermolecular interactions.

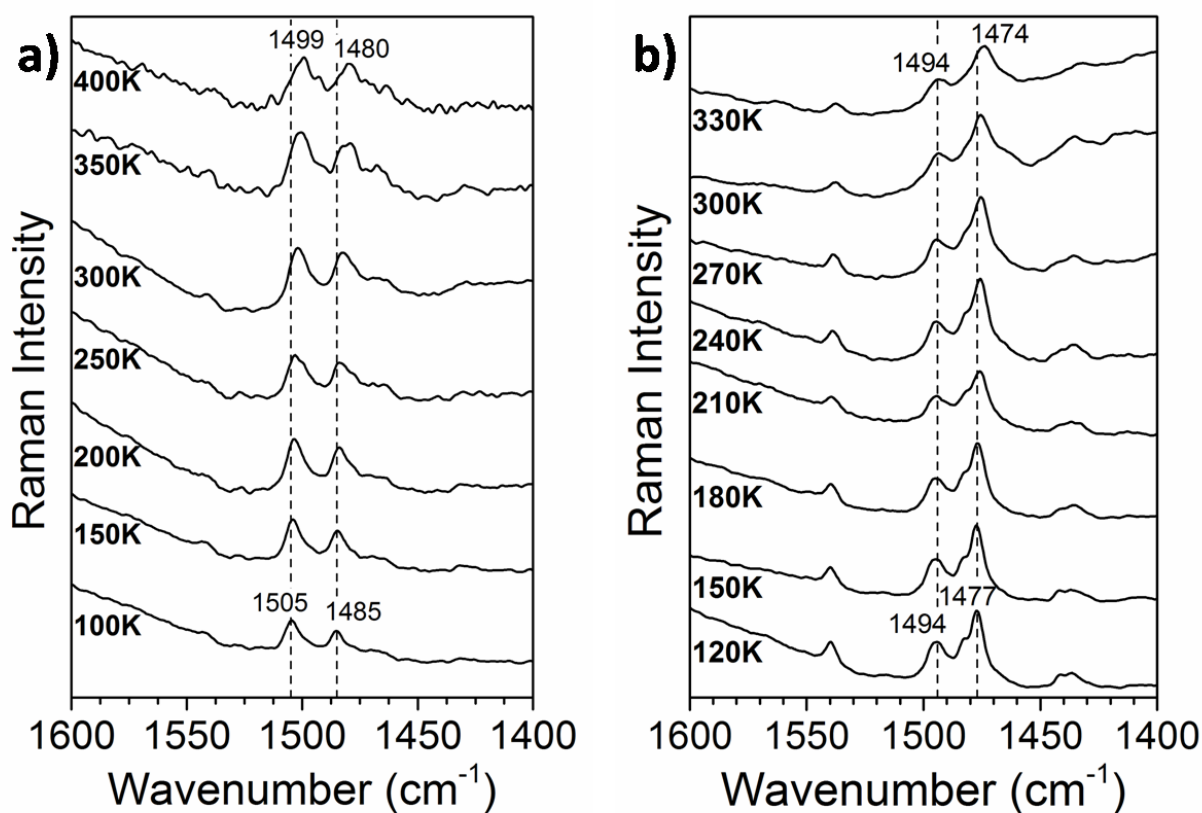


FIG. 9. Experimental Raman spectra of (a) 6TB and (b) 4T, recorded at 532 nm, at different temperatures in the  $1600\text{--}1400\text{ cm}^{-1}$  region.

The temperature-variable Raman spectra of the longer branched systems 4T and 6T have

been also investigated, with the results shown in Fig. 9. These experiments again confirm the amorphous nature of these materials. The C=C stretching modes shift upward with decreasing temperatures in both 4T and 6T systems and a shoulder at the high energy side of the strongest band at  $1477\text{ cm}^{-1}$  is observed in 4T. These changes might be associated with the alteration of the conformational distribution as intermolecular interactions might favour more planar structures not present at low temperatures.

Such temperature related effects are a prime candidate for investigation through MD simulations. However, due to the lower kinetic energy the exploration of the potential energy surface of the system will be slower, requiring significantly longer simulation times before an accurate conformational sampling can be obtained. For this reason, we presently omit such a study and instead perform rough calculations using Boltzmann weights. For the IR spectrum of B3T, the experimentally observed increase in intensity for the peak at  $1444\text{ cm}^{-1}$  was found when lowering the temperature, but the other two temperature effects marked in Fig. 8 were not present. In Fig. 10, the temperature dependence is shown for the Raman spectra of 4T and 6TB by comparing the Boltzmann weighted conformer spectra at 100 K and 300 K. While the averaged spectra do not show the clear temperature dependence that is seen in the experimental results (shifts of theoretical main peaks are as small as  $1\text{ cm}^{-1}$ ), there is a significant upward shift of individual vibrational C=C stretching modes. The populations of these vibrational states appear to be somewhat underestimated, causing their contribution to the final spectrum to be lost in the process of spectral broadening.

#### E. Further uses for MD statistics

As the MD simulations can be run before any spectrum calculation are performed, it is possible to use the information extracted from them to make the spectrum calculations more efficient. First, as has already been mentioned in Section II C, it is possible to extract representative structures for each of the conformations, giving a suitable starting point for further QM geometry optimizations. Second, as the conformational statistics are available directly from the MD trajectories, it is possible to make choices about the amount of conformations to include in the averaged spectrum. Molecules like B3T and 4T, which have 4 and 20 conformations, respectively, do not pose a great computational challenge. For 6TA and 6TB, on the other hand, which are both larger and have many more conformations, the

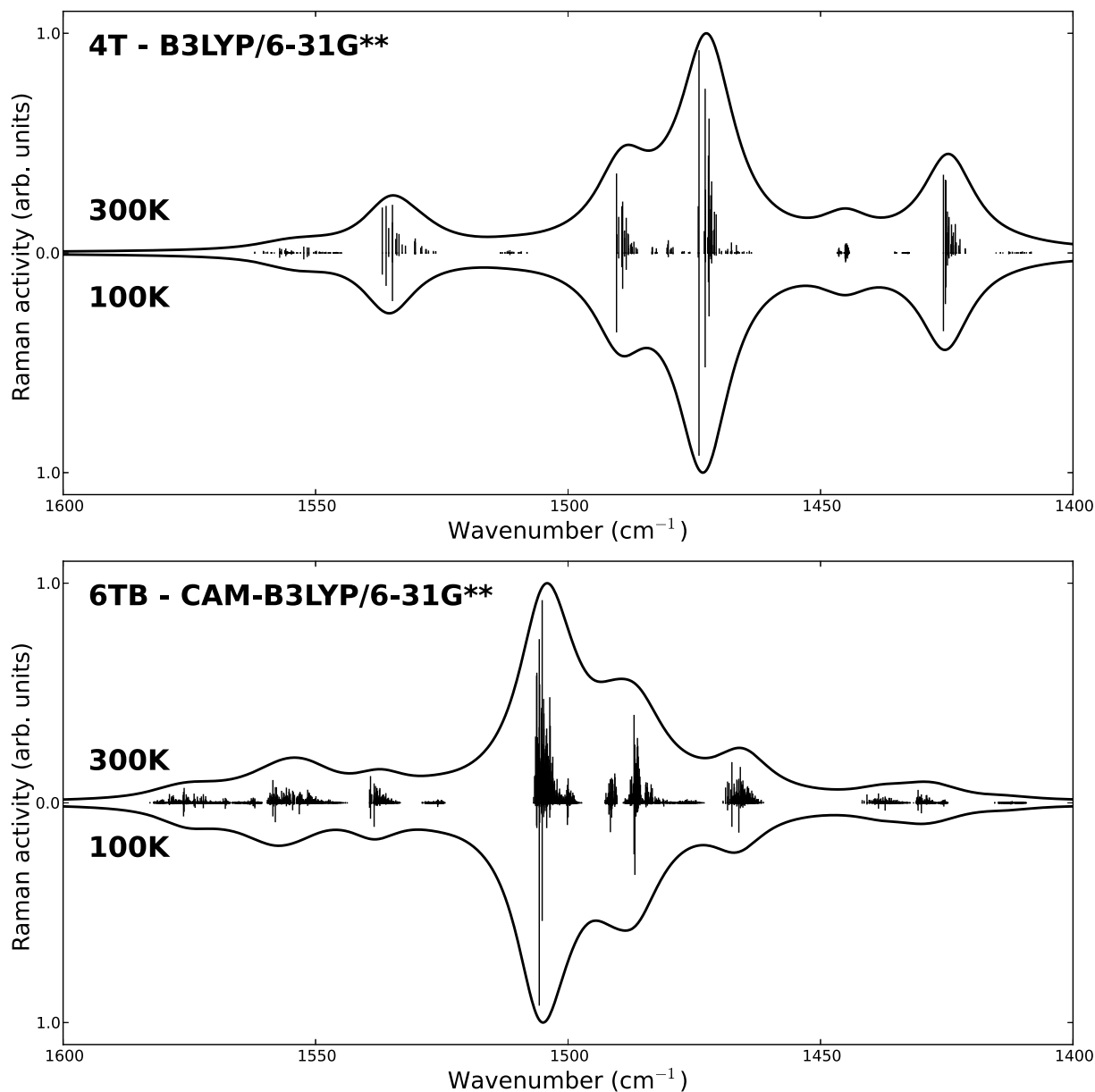


FIG. 10. Theoretical Raman spectra of 4T and 6TB, averaged using Boltzmann weights calculated for 300K and 100K. The population of the vibrational modes for all conformations are also included, weighted in the same manner as the spectra.

computational demands are much higher and it is desirable to find ways to decrease them. Both 6TA and 6TB have 272 possible conformations, but the conformational statistics show that it is quite unlikely to find the molecules in most of them. By disregarding the least likely conformations from the spectrum calculations, it is possible to drastically reduce the amount of computational resources needed. For 6TA, based on the liquid MD statistics, it

is possible to retain 95% of the weights while eliminating the 75 least likely conformations. Removing 106 conformations retains 90% of the weights while removing 149, more than half of the conformations, still leaves over 80% of the weights. Even when keeping just the 50 most likely conformations, more than 50% of the weights remain. Using this information, it is possible to choose the amount of conformations to use for the averaged spectrum based on the desired quality and the available computational resources.

## VI. CONCLUSIONS

We have presented a detailed joint theoretical and experimental vibrational study of branched oligothiophenes, as models of thiophene dendrimeric materials. The IR and Raman spectra for the molecules have been analyzed, with structural features related to spectral properties, and compared to those of the linear  $\alpha,\alpha$ -homologues.

A method for calculating theoretical vibrational spectra has been developed, where conformational statistics taken from classical molecular dynamics simulations are converted into weights for averaging individual conformer spectra. Results obtained using this method are of a quality at least as good as those obtained using traditional Boltzmann-weighting, with most being of higher quality. This method has the additional benefit of offering a path to introducing efficient computational approximations, with the possibility of discarding conformations of low weight before any spectrum calculations are performed. To accurately simulate the branched systems, parameters for the description of  $\alpha,\beta$ -linked thiophenes and 2-methylthiophenes in the CHARMM force field have been created, based on references potential energy surfaces calculated at the DFT/B3LYP level of theory.

All conformational spectra have been calculated using density functional theory, employing both the B3LYP and CAM-B3LYP functionals. Due to inadequacies in the description of long-range interactions, B3LYP is incapable of reproducing the experimental Raman spectra for the two largest molecules, 6TA and 6TB, while CAM-B3LYP fails when describing the mid-size 4T molecule.

In addition, the temperature dependence for the vibrational spectra of the branched oligothiophenes has been investigated, with the effects replicated to a lesser degree in the calculated spectra.

## VII. ACKNOWLEDGEMENTS

The work at the University of Málaga was financially supported by the MINECO of Spain (CTQ2012-33733). R.C.G.C. acknowledges the Junta de Andalucía for a personal doctoral grant. M.C.R.D. thanks the MICINN for a Ramón y Cajal Research contract. We also thank Prof. José Luis Segura and Prof. Josemon Jacob for providing us the samples under study. We acknowledge financial support from the Swedish Research Council (Grant No. 621-2010-5014) as well as a grant for computing time at National Supercomputer Centre (NSC), Sweden. M. L. thanks the Swedish e-Science Research Center (SeRC) for financial support.

- 
- \* Patrick Norman, Department of Physics, Chemistry and Biology, Linköping University, SE-581 83 Linköping, Sweden, +46-13281688, panor@ifm.liu.se
- <sup>1</sup> G. Herzberg, *Molecular Spectra and Molecular Structure. 2, Infrared and Raman spectra of Polyatomic Molecules, (Repr.)*, Krieger, Malabar, Fl., 1991[1945].
- <sup>2</sup> E. B. Wilson, J. C. Decius and P. C. Cross, *Molecular Vibrations: The Theory of Infrared and Raman Vibrational Spectra*, McGraw-Hill, New York, 1955.
- <sup>3</sup> D. A. Long, *Raman Spectroscopy*, McGraw-Hill, New York, 1977.
- <sup>4</sup> B. S. Galabov and T. Dudev, *Vibrational Intensities*, Elsevier, Amsterdam, 1996.
- <sup>5</sup> J. C. Lindon, G. E. Tranter and Holmes, J. L., *Encyclopedia of Spectroscopy and Spectrometry*, Academic Press, San Diego, 2010.
- <sup>6</sup> M. C. Ruiz Delgado, J. Casado, V. Hernández, J. T. López Navarrete, J. Orduna, B. Villacampa, R. Alicante, J.-M. Raimundo, P. Blanchard and J. Roncali, *J. Phys. Chem. C*, 2008, **112**, 3109–3120.
- <sup>7</sup> J. Casado, V. Hernández, M. C. Ruiz Delgado, R. P. Ortiz, J. T. López Navarrete, A. Facchetti and T. J. Marks, *J. Am. Chem. Soc.*, 2005, **127**, 13364–13372.
- <sup>8</sup> C. C. Ferrón, Y. Sheynin, M. Li, A. Patra, M. Bendikov, J. T. López Navarrete, V. Hernández and M. C. Ruiz Delgado, *Isr. J. Chem.*, 2014, **54**, 759–766.
- <sup>9</sup> V. Hernández, J. Casado, F. J. Ramírez, L. J. Alemany, Shu Hotta and J. T. López Navarrete, *J. Phys. Chem.*, 1996, **100**, 289–293.
- <sup>10</sup> V. Hernández, J. Casado, F. J. Ramírez, G. Zotti, Shu Hotta and J. T. López Navarrete, *J. Chem. Phys.*, 1996, **104**, 9271–9282.
- <sup>11</sup> J. Casado, S. Hotta, V. Hernández and J. T. López Navarrete, *J. Phys. Chem. A*, 1999, **103**, 816–822.
- <sup>12</sup> Y. Kim, S. A. Choulis, J. Nelson, D. D. C. Bradley, S. Cook and J. R. Durrant, *Appl. Phys. Lett.*, 2005, **86**, 063502.
- <sup>13</sup> G. Li, V. Shrotriya, J. Huang, Y. Yao, T. Moriarty, K. Emery and Y. Yang, *Nat. Mater.*, 2005, **4**, 864–868.
- <sup>14</sup> A. R. Murphy, J. Liu, C. Luscombe, D. Kavulak, J. M. J. Fréchet, R. J. Kline and M. D. McGehee, *Chem. Mater.*, 2005, **17**, 4892–4899.

- <sup>15</sup> J. Peet, J. Y. Kim, N. E. Coates, W. L. Ma, D. Moses, A. J. Heeger and G. C. Bazan, *Nat. Mater.*, 2007, **6**, 497–500.
- <sup>16</sup> C.-Q. Ma, E. Mena-Osteritz, T. Debaerdemaeker, M. M. Wienk, R. A.J. Janssen and P. Bäuerle, *Angew. Chem., Int. Ed.*, 2007, **46**, 1679–1683.
- <sup>17</sup> C.-Q. Ma, M. Fonrodona, M. C. Schikora, M. M. Wienk, R. A. J. Janssen and P. Bäuerle, *Adv. Func. Mat.*, 2008, **18**, 3323–3331.
- <sup>18</sup> H. S. Mangold, T. V. Richter, S. Link, U. Würfel and S. Ludwigs, *J. Phys. Chem. B*, 2012, **116**, 154–159.
- <sup>19</sup> J. Roncali, P. Leriche and A. Cravino, *Adv. Mater.*, 2007, **19**, 2045–2060.
- <sup>20</sup> R. C. González Cano, H. Herrera, J. L. Seguera, J. T. López Navarrete, M. C. Ruiz Delgado and J. Casado, *ChemPhysChem*, 2012, **13**, 3893–3900.
- <sup>21</sup> R. C. González Cano, G. Saini, J. Jacob, J. T. López Navarrete, J. Casado and M. C. Ruiz Delgado, *Chem. Eur. J.*, 2013, **19**, 17165–17171.
- <sup>22</sup> J. Sjöqvist, M. Linares, M. Lindgren and P. Norman, *Phys. Chem. Chem. Phys.*, 2011, **13**, 17532–17542.
- <sup>23</sup> J. Sjöqvist, M. Linares, K. V. Mikkelsen and P. Norman, *J. Phys. Chem. A*, 2014, **118**, 3419–3428.
- <sup>24</sup> A. D. MacKerell Jr., D. Bashford, M. Bellott, R. L. Dunbrack Jr., J. D. Evanseck, M. J. Field, S. Fischer, J. Gao, H. Guo, S. Ha, D. Joseph-McCarthy, L. Kuchnir, K. Kuczera, F. T. K. Lau, C. Mattos, S. Michnick, T. Ngo, D. T. Nguyen, B. Prodhom, W. E. Reiher III, B. Roux, M. Schlenkrich, J. C. Smith, R. Stote, J. Straub, M. Watanabe, J. Wiórkiewicz-Kuczera, D. Yin and M. Karplus, *J. Phys. Chem. B*, 1998, **102**, 3586–3616.
- <sup>25</sup> J. Neugebauer, M. Reiher, C. Kind and B. A. Hess, *J. Comput. Chem.*, 2002, **23**, 895–910.
- <sup>26</sup> M. J. Frisch, G. W. Trucks, H. B. Schlegel, G. E. Scuseria, M. A. Robb, J. R. Cheeseman, G. Scalmani, V. Barone, B. Mennucci, G. A. Petersson, H. Nakatsuji, M. Caricato, X. Li, H. P. Hratchian, A. F. Izmaylov, J. Bloino, G. Zheng, J. L. Sonnenberg, M. Hada, M. Ehara, K. Toyota, R. Fukuda, J. Hasegawa, M. Ishida, T. Nakajima, Y. Honda, O. Kitao, H. Nakai, T. Vreven, J. A. Montgomery, J. E. Peralta, F. Ogliaro, M. Bearpark, J. J. Heyd, E. Brothers, K. N. Kudin, V. N. Staroverov, R. Kobayashi, J. Normand, K. Raghavachari, A. Rendell, J. C. Burant, S. S. Iyengar, J. Tomasi, M. Cossi, N. Rega, N. J. Millam, M. Klene, J. E. Knox, J. B. Cross, V. Bakken, C. Adamo, J. Jaramillo, R. Gomperts, R. E. Stratmann, O. Yazyev,

- A. J. Austin, R. Cammi, C. Pomelli, J. W. Ochterski, R. L. Martin, K. Morokuma, V. G. Zakrzewski, G. A. Voth, P. Salvador, J. J. Dannenberg, S. Dapprich, A. D. Daniels, Ö. Farkas, J. B. Foresman, J. V. Ortiz, J. Cioslowski and D. J. Fox, *Gaussian 09, Revision A.02*, Gaussian, Inc., Wallingford, CT, 2004.
- <sup>27</sup> R. A. Kendall, T. H. Dunning Jr. and R. J. Harrison, *J. Chem. Phys.*, 1992, **96**, 6796–6806.
- <sup>28</sup> D. E. Woon and T. H. Dunning Jr., *J. Chem. Phys.*, 1993, **98**, 1358–1371.
- <sup>29</sup> B. Hess, C. Kutzner, D. van der Spoel and E. Lindahl, *J. Chem. Theory Comput.*, 2008, **4**, 435–447.
- <sup>30</sup> J. R. Maple, U. Dinur and A. T. Hagler, *Proc. Natl. Acad. Sci.*, 1988, **85**, 5350–5354.
- <sup>31</sup> J. R. Maple, M. J. Hwang, T. P. Stockfish, U. Dinur, M. Waldman, C. S. Ewig and A. T. Hagler, *J. Comput. Chem.*, 1994, **15**, 162–182.
- <sup>32</sup> S. Nosè, *Mol. Phys.*, 1984, **52**, 255–268.
- <sup>33</sup> S. Nosè, *J. Chem. Phys.*, 1984, **81**, 511–519.
- <sup>34</sup> W. G. Hoover, *Phys. Rev. A*, 1985, **31**, 1695–1697.
- <sup>35</sup> M. Parrinello and A. Rahman, *J. Appl. Phys.*, 1981, **52**, 7182–7190.
- <sup>36</sup> H. J. C. Berendsen, J. P. M. Postma, W. F. van Gunsteren, A. DiNola and J. R. Haak, *J. Chem. Phys.*, 1984, **81**, 3684–3690.
- <sup>37</sup> L. Martínez, R. Andrade, E. G. Birgin and J. M. Martínez, *J. Comp. Chem.*, 2009, **30**, 2157–2164.
- <sup>38</sup> G. Horowitz, B. Bachet, A. Yassar, P. Lang, F. Demanze, J.-L. Fave, F. Garnier, *Chem. Mater.*, 1995, **7**, 1337–1341.
- <sup>39</sup> T. Yanai, D. P. Tew and N. C. Handy, *Chemical Physics Letters*, 2004, **393**, 51–57.
- <sup>40</sup> W. J. Hehre, R. Ditchfield and J. A. Pople, *J. Chem. Phys.*, 1972, **56**, 2257–2261.
- <sup>41</sup> P. C. Hariharan and J. A. Pople, *Theor. Chim. Acta*, 1973, **28**, 213–222.
- <sup>42</sup> J. P. Merrick, D. Moran and L. Radom, *J. Phys. Chem. A*, 2007, **111**, 11683–11700.
- <sup>43</sup> M. E. Casida, *J. Mol. Struc. (THEOCHEM)*, 2009, **914**, 3–18.
- <sup>44</sup> F. J. Ramírez, M. A. G. Aranda, V. Hernández, J. Casado, S. Hotta and J. T. López Navarrete, *J. Chem. Phys.*, 1998, **109**, 1920–1929.